

CrossMark
click for updatesCite this: *J. Mater. Chem. A*, 2014, 2, 19696

Palladium nanoparticles immobilized on core–shell magnetic fibers as a highly efficient and recyclable heterogeneous catalyst for the reduction of 4-nitrophenol and Suzuki coupling reactions†

Xuandung Le,^a Zhengping Dong,^{*a} Yansheng Liu,^a Zhicheng Jin,^a Thanh-Do Huy,^b Minhong Le^b and Jiantai Ma^{*a}

In this study, a novel core–shell magnetic fibrous nanocatalyst, Pd/Fe₃O₄@SiO₂@KCC-1 with easily accessible active sites and a convenient recovery by applying an external magnetic field, was successfully developed. Fe₃O₄@SiO₂@KCC-1 was functionalized with amino groups which act as robust anchors so that the palladium nanoparticles (Pd NPs) with an average diameter of about 4 nm were well-dispersed on the fibers of Fe₃O₄@SiO₂@KCC-1 without obvious aggregation. The synthesized Pd/Fe₃O₄@SiO₂@KCC-1 nanocatalyst exhibited excellent catalytic activity in the reduction of 4-nitrophenol by sodium borohydride, and the Suzuki cross coupling reactions of aryl chlorides with aryl boronic acids due to the easy accessibility of the active sites. Furthermore, the Pd/Fe₃O₄@SiO₂@KCC-1 nanocatalyst was conveniently recovered by a magnet and could be reused for at least five cycles without significant loss in activity, thus confirming its good stability. Therefore, the abovementioned approach based on core–shell magnetic fibrous Fe₃O₄@SiO₂@KCC-1 provided a useful platform for the fabrication of Pd NPs based catalysts with easy accessibility, superior activity and convenient recovery.

Received 18th September 2014
Accepted 6th October 2014

DOI: 10.1039/c4ta04919e

www.rsc.org/MaterialsA

1. Introduction

In the catalytic area, noble metal nanoparticle (NMNPs) based heterogeneous catalysts have attracted significant attention due to the high catalytic efficiency in numerous liquid-phase catalytic processes.^{1–3} In particular, palladium nanoparticles (Pd NPs) based catalysts have been extensively studied because of the superior catalytic performance toward diverse reactions such as the Suzuki coupling,^{4,5} Heck C–C coupling,⁶ degradation of pollutants,⁷ hydrogenation,⁸ and fuel cells.⁹ The catalytic activity of Pd NPs is strongly dependent on the active atoms on the surface, which are usually related to the surface properties.¹⁰ Therefore, smaller Pd NPs tends to show a superior catalytic activity as it has a higher surface-to-volume ratio.^{11,12} As the size of Pd NPs reduce, the surface energy of the Pd NPs increase, thus leading to the tendency of inter-particle aggregation. The aggregation of Pd NPs reduce the catalytic efficiency of the catalysts.¹³ Therefore, the stability of the Pd NPs is another

crucial issue for their further application. One solution for Pd NP stabilization involves the use of appropriate support materials. Various supports, such as carbon,^{14,15} Al₂O₃,^{16,17} mesoporous silica,¹⁸ and core–shell magnetic mesopores,¹⁹ have been used for the immobilization of Pd NPs owing to their excellent stability, high surface areas, and robust surface chemistry. All of the abovementioned materials have large specific surface areas, which lead to the great dispersion of the NPs, thus preventing the aggregation of the NPs and improving the activity of the catalyst system. However, for all of the reported catalysts, the poor accessibility to the active sites leads to a reduction of the mass transfer effect. Silica supports with easily accessible high surface areas and not due to the pores, therefore, are highly desirable. Vivek Polshettiwar reported the synthesis of fibrous silica nanospheres (KCC-1) by the microwave assisted hydrothermal technique and our laboratory research group reported synthesis of KCC-1 by the hydrothermal method.^{20–22} Furthermore, Liu *et al.* reported the fabrication of core–shell magnetic fibrous Fe₃O₄@SiO₂@KCC-1, which have both the unique properties of KCC-1 and the physical properties of magnetic materials.²³ Therefore, Fe₃O₄@SiO₂@KCC-1 is extremely useful in the design of supported catalysts because of the unique physical properties such as easily accessible active sites, high surface area, reusability and superparamagnetism.

Recently, the transformation of harmful organic waste into reusable compounds with low toxicity in aqueous solutions

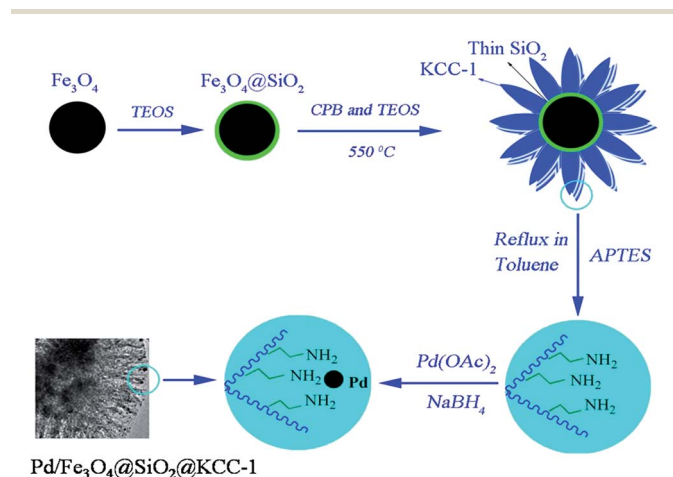
^aGansu Provincial Engineering Laboratory for Chemical Catalysis, College of Chemistry and Chemical Engineering, Lanzhou University, Lanzhou 730000, PR China. E-mail: dongzhp@lzu.edu.cn; majiantai@lzu.edu.cn; Fax: +86 931 891 2582; Tel: +86 931 891 2311

^bFaculty of Technical Physics and Chemistry, Le Quy Don Technical University, Hanoi, Vietnam

† Electronic supplementary information (ESI) available. See DOI: 10.1039/c4ta04919e

under mild conditions has become an extremely important area of study for chemists. As is well known, 4-nitrophenol (4-NP), a well-characterized industrial pollutant that has been listed on the "Priority Pollutant List" by the U.S. Environmental Protection Agency, is harmful to aquatic life and human health in terms of its toxicity, potential carcinogenicity, and mutagenicity.^{24–26} The use of the catalytic reduction process for the disposal of 4-NP is expected to be the most efficient, green, and economical method.^{27,28} In addition, considerable work has been recently directed toward the Suzuki cross coupling reaction because it is the most powerful and widely used method for the synthesis of biaryls, which are important compounds in pharmaceutical, agrochemical, natural product, and advanced materials chemistry.^{29–31} Due to the inherent advantages, several heterogeneous catalysts for the Suzuki cross coupling reaction have been developed. Particular attention is paid to the use of aryl chlorides as substrates because they are much cheaper and readily available than the usually used aryl bromides and iodides. Therefore, the catalytic activity of heterogeneous catalysts for the Suzuki cross coupling of aryl chlorides is considerably challenged. Till date, heterogeneous examples for the Suzuki cross coupling reaction of less reactive aryl chlorides are quite rare.³²

Based on the aforementioned considerations, herein, we report the synthesis of a novel core-shell magnetic fibrous Pd/Fe₃O₄@SiO₂@KCC-1 nanocatalyst system, which has the following advantages (Scheme 1): first, the Pd/Fe₃O₄@SiO₂@KCC-1 nanocatalyst exhibits high accessibility and excellent catalytic activity for the reduction of 4-NP and the Suzuki cross coupling reactions of aryl chlorides with aryl boronic acids; second, the catalyst could be easily recovered from the reaction mixture by a magnet because of the inner magnetic Fe₃O₄ core; third, the as-prepared catalyst has a long-life, because it exhibits high reusability without a visible decrease in catalytic performance after five cycles. Therefore, this study on the Pd/Fe₃O₄@SiO₂@KCC-1 nanocatalyst system provides a useful platform for exploring environmentally friendly Pd NPs based catalysts with superior activity, convenient recovery, and reusability.



Scheme 1 Preparation of the Pd/Fe₃O₄@SiO₂@KCC-1 nanocatalyst.

2. Experimental section

2.1. Materials

Tetraethoxysilane (TOES), 3-aminopropyltriethoxysilane (APTES), and Pd(II) acetate were purchased from Aladdin Chemical Co., Ltd. 4-NP, 1-pentanol, urea, and aryl halide were purchased from Lanzhou Aihua Chemical Company. Aryl boronic acids were obtained from Shanghai Chemical Reagent Co. Ltd. Organic solvents used were of analytical grade and did not require further purification.

2.2. Synthesis of Fe₃O₄ and Fe₃O₄@SiO₂ core-shell microspheres

The Fe₃O₄ NPs and Fe₃O₄@SiO₂ core-shell microspheres were synthesized according to a previously reported method.³³ FeCl₃ (2.6 g, 16 mmol), trisodium citrate (1.0 g, 3.4 mmol), and sodium acetate (NaAc) (4.0 g, 48.8 mmol) were dissolved in ethylene glycol (80 mL) with magnetic stirring. The obtained yellow solution was then transferred and sealed into a Teflon-lined stainless steel autoclave. The autoclave was heated at 200 °C for 10 h, and then allowed to cool to room temperature. The black products were isolated by strong magnetic suction, and washed with ethanol and deionized water several times.

The Fe₃O₄@SiO₂ nanospheres were prepared through a versatile solution sol-gel method as follows: the Fe₃O₄ NPs (0.7 g) was dispersed to a three-neck round-bottom flask charged with absolute ethanol (140 mL), deionized water (40 mL), and ammonia solution (3 mL, 25%) by ultrasonication for 1 h. Then the mixture was mixed for uniformity under mechanical stirring for 15 min at room temperature. Subsequently, 2.0 mL TEOS was added drop wise and the mixture was allowed to proceed for 12 h under strong mechanical stirring. The resultant core-shell Fe₃O₄@SiO₂ nanosphere product was separated by strong magnetic suction, followed by washing with ethanol and deionized water several times.

2.3. Synthesis of Fe₃O₄@SiO₂@KCC-1 core-shell microspheres

The Fe₃O₄@SiO₂@KCC-1 core-shell microspheres were synthesized according to the previously reported method (Scheme 1).²³ Fe₃O₄@SiO₂ (0.25 g) was dispersed in an aqueous solution (30 mL) containing urea (0.3 g) to form solution A under ultrasonication for 1 h. CPB (0.5 g) was added to 0.75 mL of *n*-pentanol and 30 mL cyclohexane to form solution B. Solution A was added to solution B under stirring at room temperature. Then 1.25 g TEOS was added drop wise to the abovementioned solution. The resulting mixture was continually stirred for 1 h at room temperature and then placed into a 120 °C environment for 5 h, thus inciting the reaction. After the reaction was completed, the mixture was allowed to cool to room temperature, and the Fe₃O₄@SiO₂@KCC-1 core-shell microspheres were isolated by strong magnetic suction, then washed with deionized water and acetone, and dried overnight in a drying oven at 40 °C. This material was then calcined at 550 °C for 5 h in air.

2.4. Preparation of the Pd/Fe₃O₄@SiO₂@KCC-1 nanocatalyst

The aminopropyl functionalized Fe₃O₄@SiO₂@KCC-1 nanocomposite Fe₃O₄@SiO₂@KCC-1-NH₂ was synthesized by the following procedure (Scheme 1): In a 100 mL round-bottom flask, Fe₃O₄@SiO₂@KCC-1 (0.6 g) and APTES (0.15 g) were introduced into 50 mL toluene by ultrasonication for 1 h. The mixture was refluxed for 12 h under a nitrogen protection. After cooling to room temperature, the solution was isolated by strong magnetic suction, and the solid was washed several times with ethanol to remove the remaining non-supported APTES. It was then dried in a drying oven at 40 °C overnight, from which the Fe₃O₄@SiO₂@KCC-1-NH₂ nanocomposites were obtained.

The Pd/Fe₃O₄@SiO₂@KCC-1 nanocatalyst was synthesized by the following procedure. A 100 mL round-bottom flask was charged with 0.5 g Fe₃O₄@SiO₂@KCC-1-NH₂ nanocomposite, 0.1 g Pd(OAc)₂, 30 mL deionized water, and 20 mL acetonitrile, after which it was ultrasonically dispersed for 30 min. The obtained suspension was stirred at room temperature for 2 h. Subsequently, a fresh NaBH₄ solution (0.2 M, 10 mL) was added into the abovementioned suspension. After 2 h of reduction, the product was isolated by strong magnetic suction, washed repeatedly with deionized water and ethanol, and dried overnight in a vacuum at 30 °C.

2.5. General procedure for the reduction of 4-NP

The reduction of 4-NP by NaBH₄ was chosen as a model reaction to investigate the catalytic performance of the Pd/Fe₃O₄@SiO₂@KCC-1 nanocatalyst. In short, 2.8 mL of deionized water and 30 μL of 4-NP (0.01 M) were mixed with 0.2 mL of a freshly prepared aqueous NaBH₄ solution (0.5 M), resulting in the formation of a deep yellow solution. Then, 5 μL Pd/Fe₃O₄@SiO₂@KCC-1 nanocatalyst (5 mg mL⁻¹) was added to the resulting solution, and the reaction was allowed to proceed until the solution became colorless. The reaction conversion was determined by ultraviolet visible spectroscopy (UV-Vis).

The reduction reactions were amplified 40× to characterize the reusability of the Pd/Fe₃O₄@SiO₂@KCC-1 nanocatalyst. The catalyst was recovered using a powerful magnet, washed with water and ethanol and dried in a vacuum at room temperature before being used in the next catalytic run. The 4-NP catalytic reduction process was carried out within 5 min for each cycle. This procedure was repeated five times.

2.6. General procedure for the Suzuki cross coupling reaction

After optimizing the reaction conditions (Table 2), Suzuki coupling reactions were performed by placing the aryl halide (0.5 mmol), phenyl boronic acid (0.75 mmol), K₂CO₃ (1.0 mmol), EtOH (5.0 mL), and Pd/Fe₃O₄@SiO₂@KCC-1 nanocatalyst (0.2 mol% Pd) in a 10 mL round bottom flask. The mixture was stirred at 80 °C for the required time under air. After the completion of the reaction, the mixture was cooled to room temperature and the Pd/Fe₃O₄@SiO₂@KCC-1 nanocatalyst was separated by a powerful magnet. The reaction

mixtures were analyzed by gas chromatography (GC) or GC-mass spectrometry (GC-MS).

The recovery and reuse of the Pd/Fe₃O₄@SiO₂@KCC-1 nanocatalyst is described below. A mixture of 1-iodo-4-nitrobenzene (0.5 mmol), phenyl boronic acid (0.75 mmol), K₂CO₃ (1 mmol), EtOH (5.0 mL), and Pd/Fe₃O₄@SiO₂@KCC-1 nanocatalyst (0.2 mol% Pd) was stirred at 80 °C under air. After cooling to room temperature towards the end of the reaction, the Pd/Fe₃O₄@SiO₂@KCC-1 nanocatalyst was separated by a powerful magnet. The separated catalyst was washed with ethanol and water, dried under vacuum at room temperature, and reused. The reaction mixtures were analyzed by GC or GC-MS. This procedure was repeated five times.

2.7. Characterization

The powder X-ray diffraction (XRD) spectra were obtained by a Rigaku D/max-2400 diffractometer using Cu-Kα radiation in the 2θ range of 10–90°. Fourier transform infrared (FT-IR) spectra were collected by using KBr pellets on a Nicolet Nexus 670 FT-IR spectrometer equipped with a deuterated triglycine sulfate pyroelectric detector. Transmission electron microscopy (TEM) images were obtained on a Tecnai G2 F30, FEI, USA. The UV-Vis measurement was conducted with a UV2800PC UV-Vis spectrophotometer. The magnetic measurement of Fe₃O₄@SiO₂@KCC-1 and Pd/Fe₃O₄@SiO₂@KCC-1 was performed using a quantum design vibrating sample magnetometer (VSM) at room temperature in an applied magnetic field sweeping from –15 to 15 kOe. The reaction conversion was estimated using GC (P.E. Auto System XL) or GC-MS (Shimadzu QP2010S).

3. Results and discussion

3.1. Catalyst preparation and characterization

As shown in Scheme 1, Fe₃O₄@SiO₂@KCC-1 was first functionalized with APTES, then the aminopropyl groups acted as adsorption centers for Pd²⁺. When the NaBH₄ was added to the solution, the Pd²⁺ ions were reduced and immobilized on the fibres of Fe₃O₄@SiO₂@KCC-1.

Fig. 1a shows the FT-IR spectra of Fe₃O₄@SiO₂@KCC-1 (black line) and Fe₃O₄@SiO₂@KCC-1-NH₂ (red line). The adsorption peaks at 1096 and 805 cm⁻¹ correspond to the antisymmetric and symmetric stretching vibrations of the Si–O–Si bond in the oxygen–silica tetrahedron, respectively. The peaks at 467 and 563 cm⁻¹ correspond to the Si–O and Fe–O stretching, respectively. The strong peak at 3424 cm⁻¹ shows the large number of Si–OH groups, which are proven to be advantageous for the modification of APTES on the Fe₃O₄@SiO₂@KCC-1 surface by hydrogen bonds.⁴ The adsorption peak at 2926 cm⁻¹ corresponds to the –CH stretching. In the FT-IR spectrum of Fe₃O₄@SiO₂@KCC-1-NH₂, the peak around 3400 cm⁻¹ represents the adsorption of the –OH and –NH₂ groups. The nitrogen, hydrogen, and carbon contents were 0.70%, 0.86%, and 3.20%, respectively, measured by elemental analysis. The FT-IR spectra and elemental analysis data revealed that the APTES was successfully grafted on the

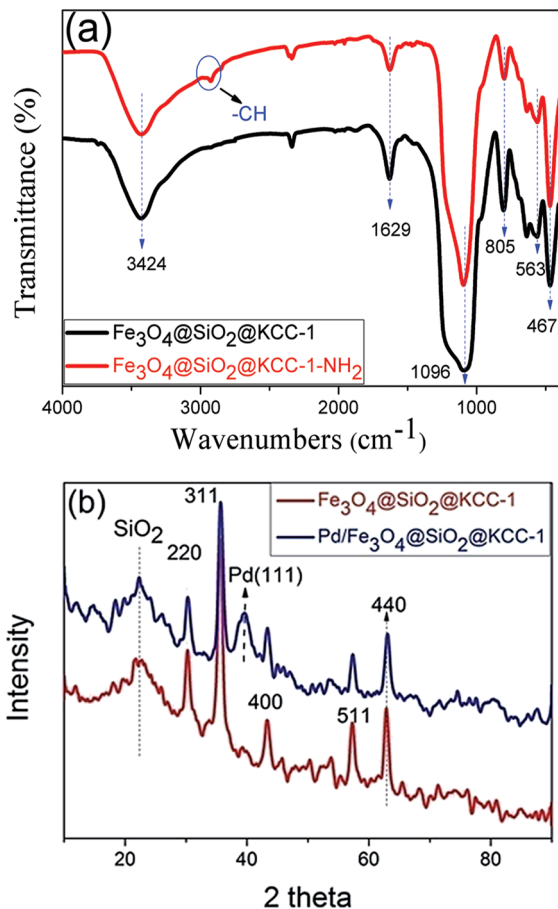


Fig. 1 (a) FT-IR spectra of $\text{Fe}_3\text{O}_4@SiO_2@KCC-1$ and $\text{Fe}_3\text{O}_4@SiO_2@KCC-1-NH_2$, (b) the XRD of $\text{Fe}_3\text{O}_4@SiO_2@KCC-1$ and $Pd/Fe_3O_4@SiO_2@KCC-1$.

$\text{Fe}_3\text{O}_4@SiO_2@KCC-1$ surface, thus enabling them to act as robust anchors for metal NPs.

The XRD patterns of the $\text{Fe}_3\text{O}_4@SiO_2@KCC-1$ and $Pd/Fe_3O_4@SiO_2@KCC-1$ samples are shown in Fig. 1b. The broad peak between 20° and 30° corresponds to amorphous silica, indicating that the silica was successfully coated on the surface of the Fe_3O_4 core. The XRD pattern of the $Pd/Fe_3O_4@SiO_2@KCC-1$ shows the characteristic peaks of magnetite NPs. The sharp and strong peaks confirm that the products are well crystallized.

The Fe_3O_4 NPs show five characteristic diffraction peaks at $2\theta = 30.3^\circ, 35.6^\circ, 43.2^\circ, 57.2^\circ,$ and 63° corresponding to (220), (311), (400), (511) and (440), respectively. The characteristic diffraction peak at 39.8° corresponds to Pd (111). The XRD pattern of $Pd/Fe_3O_4@SiO_2@KCC-1$ demonstrates that the Pd NPs were successfully immobilized on the $\text{Fe}_3\text{O}_4@SiO_2@KCC-1$ surface. The weight percentage of Pd in the $Pd/Fe_3O_4@SiO_2@KCC-1$ nanocatalyst, as determined by atomic absorption spectroscopic analysis, was 9.01 wt%.

The morphologies and structural features of the core-shell magnetic fibrous $\text{Fe}_3\text{O}_4@SiO_2@KCC-1$ and $Pd/Fe_3O_4@SiO_2@KCC-1$ nanocatalysts were analyzed by TEM. The as-prepared core-shell magnetic fibrous $\text{Fe}_3\text{O}_4@SiO_2@KCC-1$ with a fibrous structure was uniform and monodispersed (Fig. 2a). As is shown

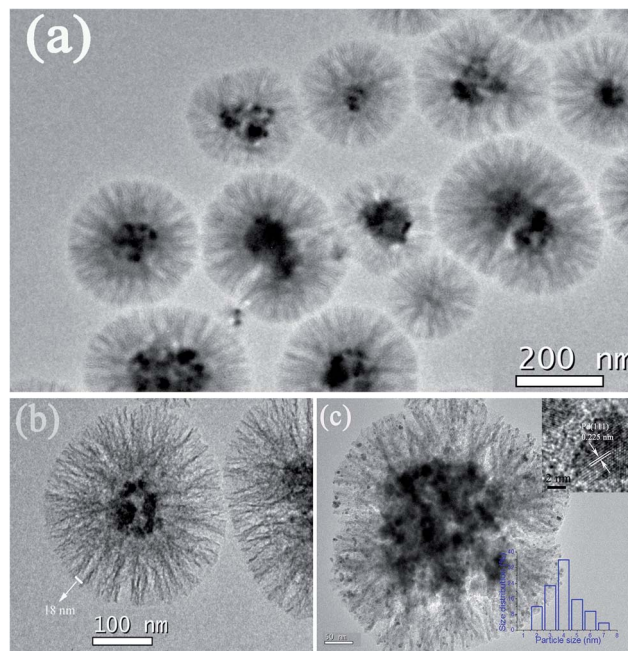


Fig. 2 (a) and (b) TEM images of $\text{Fe}_3\text{O}_4@SiO_2@KCC-1$, (c) TEM images of $Pd/Fe_3O_4@SiO_2@KCC-1$ (inset image: size distribution histogram and HRTEM image of the Pd NPs crystal structure in detail on $\text{Fe}_3\text{O}_4@SiO_2@KCC-1$).

in Fig. 2a, $\text{Fe}_3\text{O}_4@SiO_2@KCC-1$ possesses the core of Fe_3O_4 NPs and silica fibres. The average diameter of $\text{Fe}_3\text{O}_4@SiO_2@KCC-1$ and the Fe_3O_4 core were 350 nm and 100 nm, respectively. The TEM images shown in Fig. 2b further confirm that the distance between the two fibers is about 18 nm (Fig. 2b). The larger distance between the fibers leads to the easy loading of the Pd NPs on $\text{Fe}_3\text{O}_4@SiO_2@KCC-1$, resulting in the significant increase in the accessibility of the active sites on the $Pd/Fe_3O_4@SiO_2@KCC-1$ nanocatalyst. The TEM images of the $Pd/Fe_3O_4@SiO_2@KCC-1$ nanocatalyst are shown in Fig. 2c. The Pd NPs were remarkably dispersed on the surface of the core-shell magnetic fibrous $\text{Fe}_3\text{O}_4@SiO_2@KCC-1$. The Pd NPs have a narrow size distribution with a mean particle size of about 4 nm (Fig. 2c, inset). From the inset picture of Fig. 2c, it can be seen that the resolved lattice fringes of the Pd (111) planes ($d = 0.225$ nm) detected in the HRTEM image were attributed to the Pd nanocrystals.

The elemental composition of the $Pd/Fe_3O_4@SiO_2@KCC-1$ samples was determined by EDX analysis and X-ray photoelectron spectroscopy (XPS) (Fig. 3). The EDX spectrum shown in Fig. 3a reveals that the as-prepared products contain Fe, Si, Pd, Cu, C, and O, respectively. Among these elements, Cu and C are generally influenced by the copper network support films and their degree of oxidation; the Si, O, Fe and Pd signals result from the $Pd/Fe_3O_4@SiO_2@KCC-1$ nanocatalyst.

XPS was performed to investigate the chemical state of the surface of the obtained $Pd/Fe_3O_4@SiO_2@KCC-1$ nanocatalyst (Fig. 3b). The XPS elemental survey scan of the surface of the $Pd/Fe_3O_4@SiO_2@KCC-1$ nanocatalyst revealed the presence of the Si, O, Fe, Pd, N, and C elements in the samples. As shown in

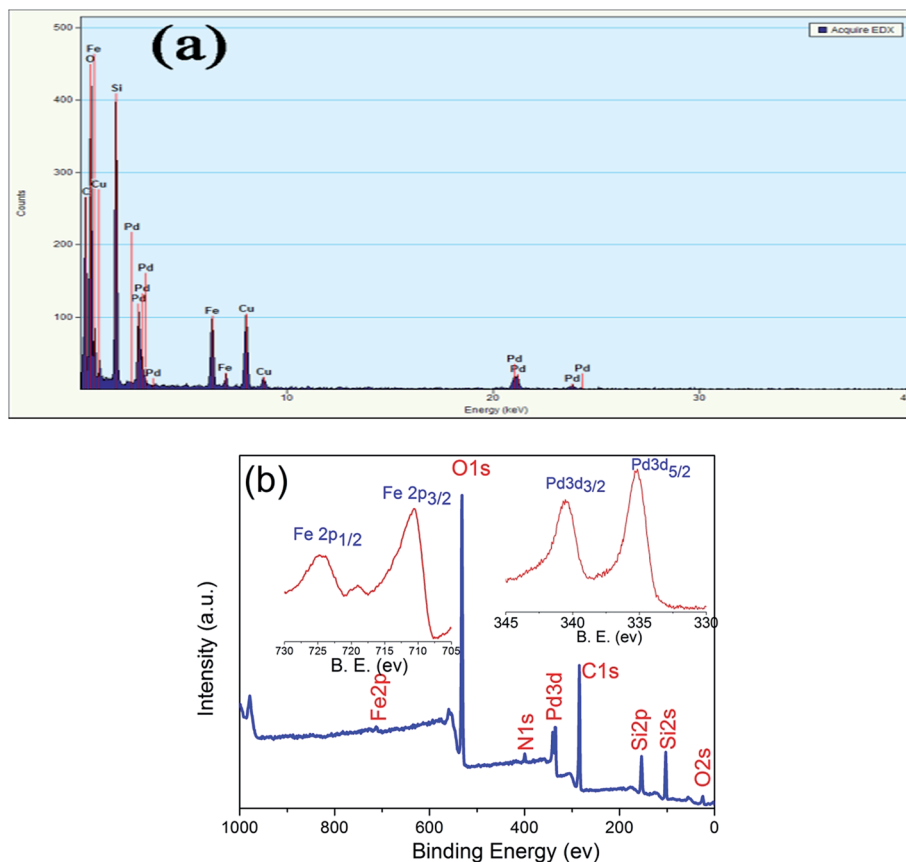


Fig. 3 (a) EDS spectrum of Pd/Fe₃O₄@SiO₂@KCC-1, (b) XPS spectrum of Pd/Fe₃O₄@SiO₂@KCC-1 (inset image: high resolution spectrum of Fe 2p and Pd 3d).

the inset of Fig. 3b, the peaks observed in the XPS spectra of Fe 2p at the binding energies of 711 and 724.5 eV are characteristic of Fe₃O₄. Moreover, the inset of Fig. 3b shows the XPS spectrum of Pd 3d_{5/2} and Pd 3d_{3/2} at the binding energies of 335 and 340.5 eV, respectively.

The magnetic measurements were carried out by VSM at room temperature. The magnetization curves measured for Fe₃O₄@SiO₂@KCC-1 and Pd/Fe₃O₄@SiO₂@KCC-1 are shown in Fig. 4. The magnetic saturation values of Fe₃O₄@SiO₂@KCC-1 and Pd/Fe₃O₄@SiO₂@KCC-1 are 20.4 and 12 emu g⁻¹, respectively. The decrease in the saturation magnetization was due to the presence of the APTES and Pd nanoparticles on the Fe₃O₄@SiO₂@KCC-1 surface. Moreover, Fig. 4 (inset image) shows the separation–redispersion process of the Pd/Fe₃O₄@SiO₂@KCC-1 nanocatalyst, which demonstrates that the catalyst is drawn from the solution to the sidewall of the vial by applying an external magnetic field. Therefore, the abovementioned results indicated an easy and efficient way to separate and recycle the Pd/Fe₃O₄@SiO₂@KCC-1 nanocatalyst from the solution by an external magnetic field.

3.2. Catalytic reduction of 4-NP

The catalytic activity of the Pd/Fe₃O₄@SiO₂@KCC-1 nanocatalyst was studied by the reduction reaction of 4-NP to 4-AP in presence of NaBH₄. The reduction process was monitored by

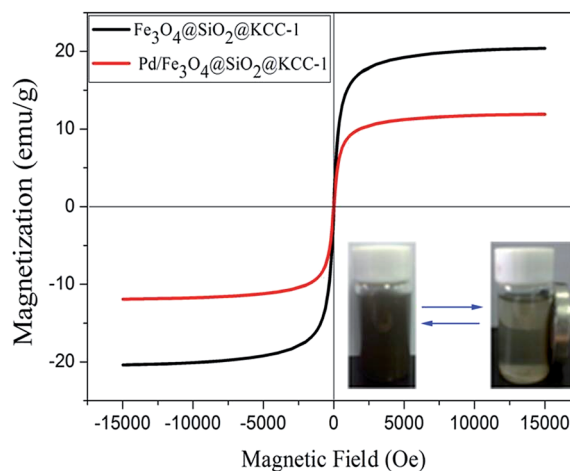


Fig. 4 Room temperature magnetization curves of the Fe₃O₄@SiO₂@KCC-1 and Pd/Fe₃O₄@SiO₂@KCC-1 nanocatalysts (inset image: the separation–redispersion process of the Pd/Fe₃O₄@SiO₂@KCC-1 nanocatalyst by an external magnetic field).

UV-Vis absorption spectroscopy. As shown in Fig. 5a, the pure 4-NP solution exhibited a distinct absorption maximum at 317 nm, which shifts to 400 nm in the presence of an alkali because of the formation of 4-nitrophenolate ions.³⁴ The reduction of 4-

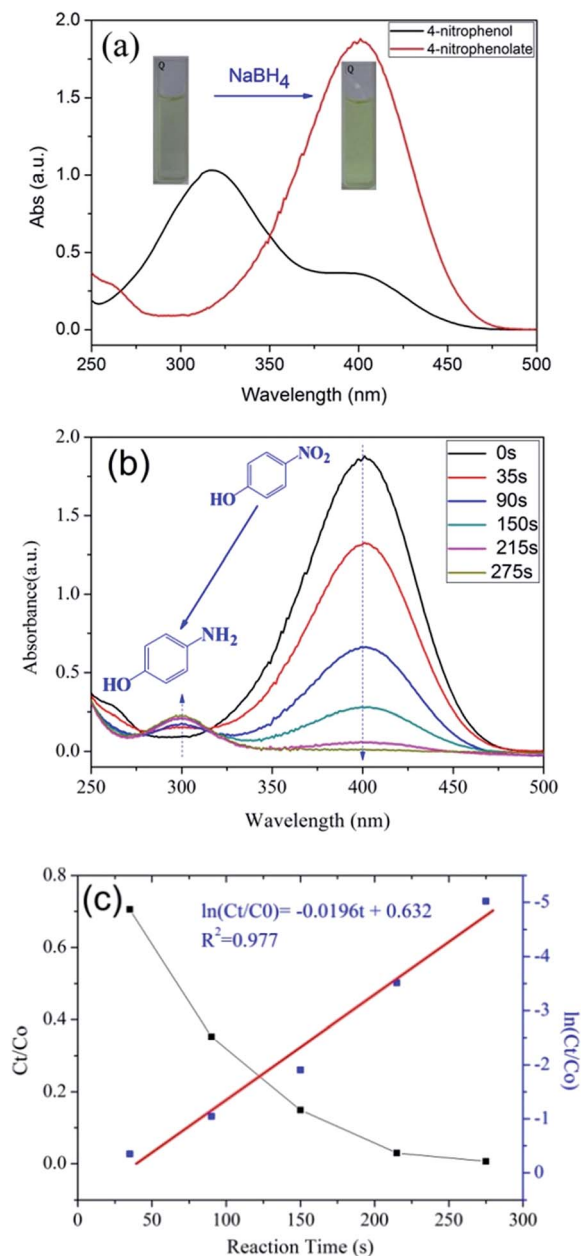


Fig. 5 (a) UV-Vis spectra of 4-NP before and after adding NaBH_4 solution, (b) the successive reduction of 4-NP to 4-AP over the prepared $\text{Pd}/\text{Fe}_3\text{O}_4@/\text{SiO}_2@/\text{KCC-1}$ nanocatalyst, (c) plot of C_t/C_0 and $\ln(C_t/C_0)$ versus reaction time for the reduction of 4-NP over $\text{Pd}/\text{Fe}_3\text{O}_4@/\text{SiO}_2@/\text{KCC-1}$.

NP to 4-AP can be obtained in the presence of NaBH_4 without any catalyst, but the time required is about 430 min.³⁵ Furthermore, when the support $\text{Fe}_3\text{O}_4@/\text{SiO}_2@/\text{KCC-1}$ was added to the 4-NP and NaBH_4 solution, it was found that, the color of the reaction mixture did not change even after 120 min, suggesting that the $\text{Fe}_3\text{O}_4@/\text{SiO}_2@/\text{KCC-1}$ support was almost inactive for the reduction reaction (Fig. S1†). Because of this, the $\text{Pd}/\text{Fe}_3\text{O}_4@/\text{SiO}_2@/\text{KCC-1}$ nanocatalyst was added in order to significantly shorten the reaction time. When the $\text{Pd}/\text{Fe}_3\text{O}_4@/\text{SiO}_2@/\text{KCC-1}$ nanocatalyst was added into the reaction mixture, the BH_4^- ions were adsorbed on the surface of the Pd NPs and

transferred a surface-hydrogen species to the surface of the Pd NPs. Simultaneously, the 4-nitrophenolate were also adsorbed on the surface of the Pd NPs resulting in the rapid occurrence and completion of the reduction reaction.^{36,37} The addition of the $\text{Pd}/\text{Fe}_3\text{O}_4@/\text{SiO}_2@/\text{KCC-1}$ nanocatalyst into the reaction mixture led to the decrease in the peak intensity of the 4-nitrophenolate ion at 400 nm with a concomitant increase in the peaks corresponding to 4-AP at 300 nm (Fig. 5b), reflecting the decay of 4-NP and formation of 4-AP. Thus, the conversion of 4-NP to 4-AP can be monitored by tracking the changes in the absorbance peak of the 4-nitrophenolate ions at 400 nm.³⁸ The absorbance peak value of 4-nitrophenolate ions at 400 nm decreased to zero, indicating the successful conversion of 4-NP to 4-AP. Fig. 5b shows the complete reduction of 4-NP to 4-AP after 275 seconds. The concentration of NaBH_4 was very high compared with that of 4-NP, and the reaction followed pseudo-first-order reaction kinetics.²² Therefore, we used pseudo-first-order kinetics to evaluate the kinetic rate constant (k_{app}) of the current reaction [eqn (1)]. The reaction conversion was calculated from C_t/C_0 (Fig. 5c), which was measured using the relative intensity of the UV-Vis absorbance (A_t/A_0) at 400 nm. C_t and C_0 are the concentrations of the 4-NP at reaction time t and the initial stage, respectively.

$$dC_t/dt = -k_{\text{app}}t, \text{ or } \ln(C_t/C_0) = \ln(A_t/A_0) = -k_{\text{app}}t \quad (1)$$

As shown in Fig. 5c, the linear correlation between $\ln(C_t/C_0)$ and reaction time (t) was confirmed through pseudo-first-order kinetics. We calculated the apparent kinetic rate constant k_{app} to be 1.96×10^{-2} for the $\text{Pd}/\text{Fe}_3\text{O}_4@/\text{SiO}_2@/\text{KCC-1}$ catalyzed reductions of 4-NP. Then, k_{app} was normalized to the concentration of Pd, deriving k_{nor} to reveal the intrinsic catalytic activity of the catalyst ($k_{\text{nor}} = k_{\text{app}}/c_{\text{Pd}}$).¹⁴ We compared the activity of $\text{Pd}/\text{Fe}_3\text{O}_4@/\text{SiO}_2@/\text{KCC-1}$ with Pd catalysts loaded on different supports for the reduction of 4-NP (Table 1). In Table 1, $\text{Pd}/\text{Fe}_3\text{O}_4@/\text{SiO}_2@/\text{KCC-1}$ shows excellent catalytic activity for the reduction of 4-NP by NaBH_4 , with the highest k_{nor} ($2.78 \text{ s}^{-1} \text{ mM}^{-1}$) among the Pd catalysts loaded on different supports: SBA-15,³⁹ PEDOT (conducting polymer),⁴⁰ Microgel-PS (microgel coated polystyrene),⁴¹ FG (functionalized graphene nano-hybrids),⁴² PiHP (hyper-branched polymer),⁴³ and Al_2O_3 .⁴⁴ It is also higher than the Pd nanoclusters⁴⁵ and Pd nanocrystals⁴⁶ based catalysts. The excellent catalytic activity of the $\text{Pd}/\text{Fe}_3\text{O}_4@/\text{SiO}_2@/\text{KCC-1}$ nanocatalyst is owed to the ease of access of its active sites, and the low aggregation of the Pd NPs on the $\text{Fe}_3\text{O}_4@/\text{SiO}_2@/\text{KCC-1}$ support. In this situation, the reactant can be easily adsorbed on the Pd NPs surface, which allows the reduction reaction to start quickly and finish rapidly.

3.3. Catalyst testing for the Suzuki cross coupling reaction

The abovementioned results revealed that the $\text{Pd}/\text{Fe}_3\text{O}_4@/\text{SiO}_2@/\text{KCC-1}$ nanocatalyst exhibited excellent properties for the reduction of 4-NP. We further explored the catalytic activity of the $\text{Pd}/\text{Fe}_3\text{O}_4@/\text{SiO}_2@/\text{KCC-1}$ nanocatalyst for the Suzuki cross coupling reactions. To explore the optimal reaction conditions, a series of reactions was performed using several time

Table 1 Comparison of the apparent kinetic rate constant (k_{app}) and normalized rate constants (k_{nor}) of Pd catalysts loaded on different supports for the reduction of 4-NP

Samples	$c_{(4\text{-NP})}^a$ (mM)	$c_{(\text{Pd})}^a$ (mM)	k_{app}^b (s^{-1})	k_{nor}^c ($\text{s}^{-1} \text{mM}^{-1}$)	Ref.
Pd/SBA-15	0.1	6.29×10^{-2}	11.8×10^{-3}	0.118	39
Pd/PEDOT		2.52×10^{-1}	65.8×10^{-3}	0.261	40
Pd/microgel-PS	0.1	2.15×10^{-3}	1.50×10^{-3}	0.698	41
Pd/FG	5.8×10^{-2}	4.72×10^{-3}	2.35×10^{-3}	0.498	42
Pd nanoclusters	2	1.6	7.89×10^{-4}	0.005	45
Pd/PiHP	2.3	9×10^{-2}	20×10^{-3}	0.222	43
Pd nanocrystals	8×10^{-2}	3.6×10^{-2}	4.83×10^{-3}	0.134	46
Pd/ Al_2O_3	0.1	8.48×10^{-3}	9.2×10^{-3}	1.085	44
Pd/ $\text{Fe}_3\text{O}_4@/\text{SiO}_2@/\text{KCC-1}$	0.1	7.06×10^{-3}	19.6×10^{-3}	2.78	This work

^a c : concentration. ^b k_{app} : apparent rate constant. ^c k_{nor} : rate constant normalized to the molar concentration of Pd. Data were given or calculated in the respective papers; some data were not obtained.

durations, solvents, bases, and temperatures to obtain the best possible combination. Initially, the experiments were performed using the Suzuki cross-coupling reaction of 1-iodo-4-nitrobenzene (0.5 mmol) with phenyl boronic acid (0.75 mmol) in presence of Pd/ $\text{Fe}_3\text{O}_4@/\text{SiO}_2@/\text{KCC-1}$ (0.2% Pd) and 5 mL ethanol in air at 80 °C for 1 h, 2 h, and 3 h. The corresponding products were obtained in the following yields: 91.0%, 94.0%, and 97%, respectively (Table 2: entries 1–3). The reaction product with the highest yield was obtained at 3 h, therefore the reaction time of 3 h was chosen. As it is known, the solvent plays a crucial role in the rate of Suzuki coupling reactions. When the reactions were carried out in methyl alcohol, ethyl acetate, deionized water, and acetone under the same conditions, the products were obtained in poor to moderate yields of 85.0%, 79.6%, 27.8%, and 30%, respectively (Table 2: entries 4–7). The reactions were carried out under similar conditions using different bases such as K_2CO_3 , CH_3COONa , NaOH, and $(\text{C}_2\text{H}_5)_3\text{N}$; the yields were 97%, 80.3%, 90.1%, and 80.9%,

respectively (Table 2: entries 3, 8–10). For the reactions at room temperature, 40 °C, and 60 °C corresponding products were obtained in the following yields: 54%, 78.8%, and 90.8% (Table 2: entries 11–13). The best catalytic activity of the Pd/ $\text{Fe}_3\text{O}_4@/\text{SiO}_2@/\text{KCC-1}$ nanocatalyst was observed using ethanol as the solvent, and K_2CO_3 as the base at 80 °C (Table 2: entry 3).

After screening the reaction conditions, the catalyst system was studied for the Suzuki cross coupling reaction of various aryl halides and aryl boronic acids (Table 3). As listed in Table 3, when the coupling of aryl iodides with aryl boronic acids proceeded at 80 °C for 3 h, the corresponding products were obtained in high yields (Table 3: entries 1–8). The Pd/ $\text{Fe}_3\text{O}_4@/\text{SiO}_2@/\text{KCC-1}$ nanocatalyst also revealed excellent catalytic activity for the coupling between aryl bromides and aryl boronic acids as the reaction time approached 6 h (Table 3: entries 9–18). However, for the reactions of 1-bromo-2-nitrobenzene, poor yields (Table 3, entries 13 and 18) were obtained due to the electron-withdrawing $-\text{NO}_2$ group in the *ortho* position. It is

Table 2 The effects of solvent, base and temperature on the Suzuki cross coupling of 1-iodo-4-nitrobenzene with phenyl boronic acid using the Pd/ $\text{Fe}_3\text{O}_4@/\text{SiO}_2@/\text{KCC-1}$ nanocatalyst

Entry	Solvent	Base	Temp (°C)	Time (h)	Yield (%)
1	Ethanol	K_2CO_3	80	1	91.0
2	Ethanol	K_2CO_3	80	2	94.0
3	Ethanol	K_2CO_3	80	3	97.0
4	Methyl alcohol	K_2CO_3	80	3	85.0
5	Ethyl acetate	K_2CO_3	80	3	79.6
6	Deionized water	K_2CO_3	80	3	27.8
7	Acetone	K_2CO_3	80	3	30.0
8	Ethanol	CH_3COONa	80	3	80.3
9	Ethanol	NaOH	80	3	90.1
10	Ethanol	$(\text{C}_2\text{H}_5)_3\text{N}$	80	3	80.9
11	Ethanol	K_2CO_3	25	3	54.0
12	Ethanol	K_2CO_3	40	3	78.8
13	Ethanol	K_2CO_3	60	3	90.8

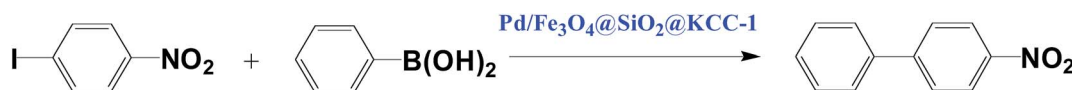


Table 3 Suzuki cross coupling reactions of aryl halides with aryl boronic acids using the Pd/Fe₃O₄@SiO₂@KCC-1 nanocatalyst^a

Entry	Aryl halide	Aryl boronic acid	Time (h)	Yield (%)
1			3	98.9
2			3	96.8
3			3	99.0
4			3	96.0
5			3	99.0
6			3	97.8
7			3	99.0
8			3	97.0
9			6	89.0
10			6	91.8
11			6	90.6
12			6	86.8
13			6	26.2
14			6	90.8
15			6	93.2
16			6	91.8
17			6	87.3
18			6	28.1

^a Reaction condition: aryl halide (0.5 mmol), aryl boronic acid (0.75 mmol), K₂CO₃ (1.0 mmol), EtOH 5.0 mL, Pd/Fe₃O₄@SiO₂@KCC-1 nanocatalyst (0.2 mol% of Pd), and 80 °C, in air. Yield was determined by GC-MS or GC analysis.

noteworthy that aryl iodides and aryl bromides containing electron-donating groups, such as $-\text{CH}_3$, $-\text{OH}$, $-\text{NH}_2$ were found to be more active than the aryl iodides and aryl bromides containing electron-withdrawing groups, such as $-\text{NO}_2$ (Table 3).

Although the catalyst was active for aryl iodides and aryl bromides, our main objective was to design a nanocatalyst for the Suzuki coupling of challenging substrates, that is, the Suzuki coupling reactions of aryl chlorides with aryl boronic acids. In our initial attempts, we used the same optimized conditions for the aryl iodides and aryl bromides, but the products were obtained in low yields.

Therefore, we optimized several reaction parameters, including the solvent, reaction temperature mentioned in previously studied reports,^{47,48} and found that the use of tetra-*n*-butylammonium bromide (TBAB) and changing the solvent from ethanol to (*n*-methyl-2-pyrrolidone) NMP and raising the reaction temperature to 140 °C was necessary to achieved good yields. After optimizing the reaction conditions, the Pd/Fe₃O₄@SiO₂@KCC-1 nanocatalyst was studied for Suzuki cross coupling reactions of several aryl chlorides with aryl boronic acids, which are summarized in Table 4.

Interestingly, the Pd/Fe₃O₄@SiO₂@KCC-1 nanocatalyst also revealed excellent catalytic activity for the Suzuki coupling

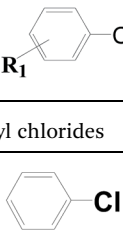
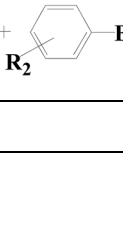
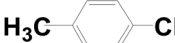
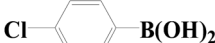
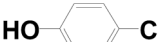
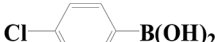
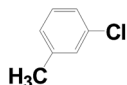
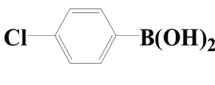
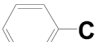

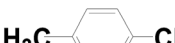
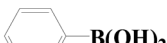
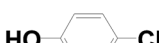

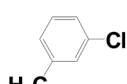
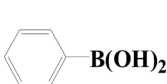
between aryl chlorides and aryl boronic acids. Few heterogeneous catalyst systems show good activity toward aryl chlorides. The highly dispersed smaller Pd NPs with easily accessible active sites, are sustainable substrates for Suzuki cross coupling reactions, under ligand-free conditions.⁴⁹

3.4. Reusability of the Pd/Fe₃O₄@SiO₂@KCC-1 nanocatalyst

For the practical application of heterogeneous systems, the recyclability of the catalyst is an important factor. The stability and reusability of the Pd/Fe₃O₄@SiO₂@KCC-1 nanocatalyst were performed by catalyzing the reduction of 4-NP and the Suzuki coupling reaction of 1-iodo-4-nitrobenzene with phenyl boronic acid.

As shown in Fig. 6, the recovered Pd/Fe₃O₄@SiO₂@KCC-1 nanocatalyst exhibited almost constant catalytic activity for at least five successive cycles in the reduction of 4-NP and Suzuki cross coupling reaction of 1-iodo-4-nitrobenzene with phenyl boronic acid. Moreover, the catalyst was easily separated magnetically from the reaction mixture, washed with ethanol and deionized water, and finally dried for the next run. This result suggests that the Pd/Fe₃O₄@SiO₂@KCC-1 nanocatalyst possesses robust stability.

Table 4 The Suzuki cross coupling reactions of aryl chlorides with aryl boronic acids using the Pd/Fe₃O₄@SiO₂@KCC-1 nanocatalyst^a

Entry	Aryl chlorides	Aryl boronic acid	Time (h)	Yield (%)
1			12	83.2
2			12	86.0
3			12	85.8
4			12	80
5			12	83.8
6			12	87.8
7			12	86.2
8			12	79.8

^a Reaction conditions: aryl chlorides (0.5 mmol), aryl boronic acid (0.75 mmol), K₂CO₃ (1.0 mmol) were added in 5 mL NMP at 140 °C for 12 h in the presence of TBAB (0.05 mmol) and Pd/Fe₃O₄@SiO₂@KCC-1 (2.5 mol% of Pd). Yield was determined by GC-MS or GC.

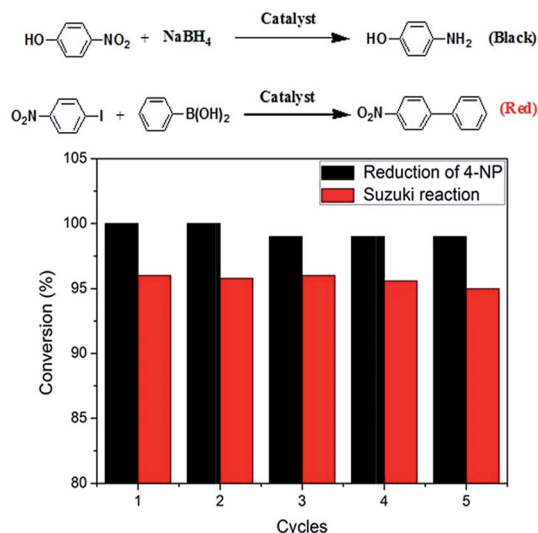


Fig. 6 The reusability of the Pd/Fe₃O₄@SiO₂@KCC-1 nanocatalyst for the reduction of 4-NP by NaBH₄ and Suzuki cross coupling reaction of 1-iodo-4-nitrobenzene with phenyl boronic acid.

4. Conclusion

In this study, a novel core-shell magnetic fibrous Fe₃O₄@SiO₂@KCC-1 based Pd/Fe₃O₄@SiO₂@KCC-1 nanocatalyst with easily accessible active sites was successfully synthesized. The catalyst could be easily recovered by applying an external magnetic field, and reused for next catalytic run. The Pd/Fe₃O₄@SiO₂@KCC-1 nanocatalyst showed excellent catalytic activity for the reduction of 4-NP and the Suzuki coupling reaction for a range of aryl bromides and iodides with aryl boronic acids. Notably, the catalyst also displayed good catalytic activity for the Suzuki coupling reaction of aryl chlorides with aryl boronic acids. Moreover, the catalyst was chemically stable and could be easily recycled for at least five times in the corresponding reaction without reduction in the catalytic activity. The Pd/Fe₃O₄@SiO₂@KCC-1 nanocatalyst acts as a relatively green catalyst with superparamagnetism, eco-friendly nature and convenient recovery, and is a promising candidate for Pd NPs based catalytic applications in industrial syntheses.

Acknowledgements

The authors acknowledge the financial support from the NSFC (Grants 21301082) and the Natural Science Foundation of Gansu (no. 1308RJYA028).

References

- S. Paganelli, O. Piccolo, F. Baldi, R. Tassini, M. Gallo and G. La Sorella, *Appl. Catal., A*, 2013, **451**, 144–152.
- Y. Shiraishi, K. Fujiwara, Y. Sugano, S. Ichikawa and T. Hirai, *ACS Catal.*, 2013, **3**, 312–320.
- K. Imamura, T. Yoshikawa, K. Nakanishi, K. Hashimoto and H. Kominami, *Chem. Commun.*, 2013, **49**, 10911–10913.

- X. Le, Z. Dong, Z. Jin, Q. Wang and J. Ma, *Catal. Commun.*, 2014, **53**, 47–52.
- P. Wang, H. Liu, J. Niu, R. Li and J. Ma, *Catal. Sci. Technol.*, 2014, **4**, 1333–1339.
- F. Zhang, J. Jin, X. Zhong, S. Li, J. Niu, R. Li and J. Ma, *Green Chem.*, 2011, **13**, 1238–1243.
- M.-Q. Yang, X. Pan, N. Zhang and Y.-J. Xu, *CrystEngComm*, 2013, **15**, 6819–6828.
- Z. Dong, X. Le, C. Dong, W. Zhang, X. Li and J. Ma, *Appl. Catal., B*, 2015, **162**, 372–380.
- E. Antolini, *Energy Environ. Sci.*, 2009, **2**, 915–931.
- H. Lee, S. E. Habas, S. Kweskin, D. Butcher, G. A. Somorjai and P. Yang, *Angew. Chem., Int. Ed.*, 2006, **45**, 7824–7828.
- J. Zeng, Q. Zhang, J. Chen and Y. Xia, *Nano Lett.*, 2009, **10**, 30–35.
- M.-L. Wang, T.-T. Jiang, Y. Lu, H.-J. Liu and Y. Chen, *J. Mater. Chem. A*, 2013, **1**, 5923–5933.
- Y. Lin, Y. Qiao, Y. Wang, Y. Yan and J. Huang, *J. Mater. Chem.*, 2012, **22**, 18314–18320.
- Y. Fang and E. Wang, *Nanoscale*, 2013, **5**, 1843–1848.
- D. Ganapathy and G. Sekar, *Catal. Commun.*, 2013, **39**, 50–54.
- G. Feng, F. Liu, C. Lin, W. Li, S. Wang and C. Qi, *Catal. Commun.*, 2013, **37**, 27–31.
- G. Yuan and M. A. Keane, *Ind. Eng. Chem. Res.*, 2007, **46**, 705–715.
- S. Wei, Z. Ma, P. Wang, Z. Dong and J. Ma, *J. Mol. Catal. A: Chem.*, 2013, **370**, 175–181.
- W. Li, B. Zhang, X. Li, H. Zhang and Q. Zhang, *Appl. Catal., A*, 2013, **459**, 65–72.
- V. Polshettiwar, D. Cha, X. Zhang and J. M. Basset, *Angew. Chem., Int. Ed.*, 2010, **49**, 9652–9656.
- A. Fihri, M. Bouhrara, U. Patil, D. Cha, Y. Saih and V. Polshettiwar, *ACS Catal.*, 2012, **2**, 1425–1431.
- Z. Dong, X. Le, X. Li, W. Zhang, C. Dong and J. Ma, *Appl. Catal., B*, 2014, **158–159**, 129–135.
- K. Yu, X. Zhang, H. Tong, X. Yan and S. Liu, *Mater. Lett.*, 2013, **106**, 151–154.
- Y. C. Chang and D. H. Chen, *J. Hazard. Mater.*, 2009, **165**, 664–669.
- J.-R. Chiou, B.-H. Lai, K.-C. Hsu and D.-H. Chen, *J. Hazard. Mater.*, 2013, **248**, 394–400.
- K. Li, Z. Zheng, X. Huang, G. Zhao, J. Feng and J. Zhang, *J. Hazard. Mater.*, 2009, **166**, 213–220.
- Y. Zhang, X. Yuan, Y. Wang and Y. Chen, *J. Mater. Chem.*, 2012, **22**, 7245–7251.
- S. Saha, A. Pal, S. Kundu, S. Basu and T. Pal, *Langmuir*, 2010, **26**, 2885–2893.
- N. Miyaura and A. Suzuki, *Chem. Rev.*, 1995, **95**, 2457–2483.
- A. Suzuki, *J. Organomet. Chem.*, 1999, **576**, 147–168.
- P. Wang, F. Zhang, Y. Long, M. Xie, R. Li and J. Ma, *Catal. Sci. Technol.*, 2013, **3**, 1618–1624.
- H. Yang, G. Li and Z. Ma, *J. Mater. Chem.*, 2012, **22**, 6639–6648.
- Y. Deng, Y. Cai, Z. Sun, J. Liu, C. Liu, J. Wei, W. Li, C. Liu, Y. Wang and D. Zhao, *J. Am. Chem. Soc.*, 2010, **132**, 8466–8473.

- 34 K. Kim, K. L. Kim and K. S. Shin, *J. Phys. Chem. C*, 2011, **115**, 14844–14851.
- 35 T. Wu, L. Zhang, J. Gao, Y. Liu, C. Gao and J. Yan, *J. Mater. Chem. A*, 2013, **1**, 7384–7390.
- 36 B. Baruah, G. J. Gabriel, M. J. Akbashev and M. E. Booher, *Langmuir*, 2013, **29**, 4225–4234.
- 37 D. H. Lee, S. O. Kim and W. J. Lee, *J. Phys. Chem. C*, 2010, **114**, 8114.
- 38 X. Le, Z. Dong, W. Zhang, X. Li and J. Ma, *J. Mol. Catal. A: Chem.*, 2014, **395**, 58–65.
- 39 J. Morere, M. J. Tenorio, M. J. Torralvo, C. Pando, J. A. R. Renuncio and A. Cabanas, *J. Supercrit. Fluids*, 2011, **56**, 213–222.
- 40 S. Harish, J. Mathiyarasu, K. L. N. Phani and V. Yegnaraman, *Catal. Lett.*, 2009, **128**, 197–202.
- 41 Y. Mei, Y. Lu, F. Polzer, M. Ballauff and M. Drechsler, *Chem. Mater.*, 2007, **19**, 1062–1069.
- 42 Z. Wang, C. Xu, G. Gao and X. Li, *RSC Adv.*, 2014, **4**, 13644–13651.
- 43 H. Li, L. Han, J. Cooper-White and I. Kim, *Green Chem.*, 2012, **14**, 586–591.
- 44 S. Arora, P. Kapoor and M. Singla, *React. Kinet., Mech. Catal.*, 2010, **99**, 157–165.
- 45 A. Halder, S. Patra, B. Viswanath, N. Munichandraiah and N. Ravishankar, *Nanoscale*, 2011, **3**, 725–730.
- 46 G. Fu, X. Jiang, L. Ding, L. Tao, Y. Chen, Y. Tang, Y. Zhou, S. Wei, J. Lin and T. Lu, *Appl. Catal., B*, 2013, **138–139**, 167–174.
- 47 A. Fihri, D. Cha, M. Bouhrara, N. Almana and V. Polshettiwar, *ChemSusChem*, 2012, **5**, 85–89.
- 48 A. Indra, C. S. Gopinath, S. Bhaduri and G. Kumar Lahiri, *Catal. Sci. Technol.*, 2013, **3**, 1625–1633.
- 49 A. Fihri, M. Bouhrara, B. Nekouei-shahraki, J.-M. Basset and V. Polshettiwar, *Chem. Soc. Rev.*, 2011, **40**, 5181–5203.